ACS APPLIED MATERIALS & INTERFACES

Research Article

www.acsami.org

Modeling Mechanochemical Reaction Mechanisms

Heather Adams,[†] Brendan P. Miller,[‡] Octavio J. Furlong,[§] Marzia Fantauzzi,[∥,⊥] Gabriele Navarra,[∥,⊥] Antonella Rossi,[∥,⊥] Yufu Xu,[#] Peter V. Kotvis,[†] and Wilfred T. Tysoe*[,†]

[†]Department of Chemistry and Laboratory for Surface Studies, University of Wisconsin—Milwaukee, Milwaukee, Wisconsin 53211, United States

[‡]Chevron Oronite Company, LLC., 100 Chevron Way, Richmond, California 94802, United States

[§]INFAP/CONICET, Universidad Nacional de San Luis, Ejército de los Andes 950, 5700 San Luis, Argentina

[∥]Dipartimento di Scienze Chimiche e Geologiche, Università degli Studi di Cagliari, Campus di Monserrato S.S. 554, Cagliari 09124, Italy

[⊥]INSTM, UdR, Cagliari 09100 Italy

[#]Institute of Tribology, School of Mechanical and Automotive Engineering, Hefei University of Technology, Hefei 230009, China

Supporting Information

ABSTRACT: The mechanochemical reaction between copper and dimethyl disulfide is studied under well-controlled conditions in ultrahigh vacuum (UHV). Reaction is initiated by fast S−S bond scission to form adsorbed methyl thiolate species, and the reaction kinetics are reproduced by two subsequent elementary mechanochemical reaction steps, namely a mechanochemical decomposition of methyl thiolate to deposit sulfur on the surface and evolve small, gas-phase hydrocarbons, and sliding-induced oxidation of the copper by sulfur that regenerates vacant reaction sites. The steady-state reaction kinetics are monitored in situ from the variation in the friction force as the reaction proceeds and modeled using the elementary-step reaction rate constants found for monolayer adsorbates. The analysis yields excellent agreement between the experiment and the kinetic model, as well as correctly predicting the total amount of subsurface sulfur in the film measured using Auger spectroscopy and the sulfur depth distribution measured by angle-resolved X-ray photoelectron spectroscopy.

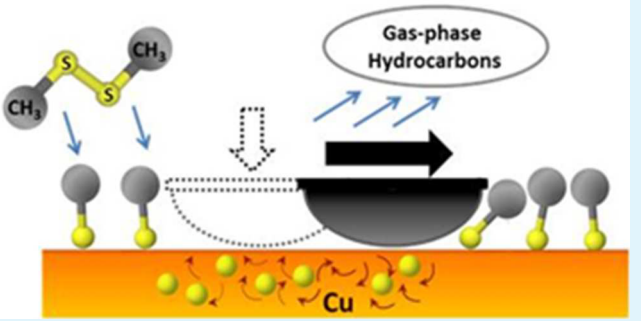

KEYWORDS: *dialkyl disulfides, copper, mechanochemistry, XPS, in situ analysis, Auger spectroscopy*

INTRODUCTION

While mechanochemical reactions have been known for millennia,[1] and were studied in the 19th century,[2] there is currently little understanding of their reaction pathways and the effects that control them.[3] Despite this lack of fundamental understanding, a significant number of mechanochemical synthetic methods have been developed empirically over the past decades.[4−16]

Mechanochemical effects have been studied on the molecular scale by exploiting the exquisite force sensitivity of atomic force microscopy (AFM) to pull single molecules.[17−25] While these experiments provide detailed information on how forces accelerate the rates of single-bond scission of a mechanically active center (a mechanophore), they provide little information on mechanochemical reaction pathways. This is addressed here by studying a simple, model mechanochemical reaction between dimethyl disulfide (DMDS) and copper to form gas-phase hydrocarbons and copper sulfide under well-controlled conditions induced by sliding on a planar copper substrate. This approach has several advantages; the presence of the surface allows well-defined forces to be applied to the anchored mechanophore and enables the kinetics of the elementary-step reactions to be followed.

Such sulfur-containing molecules are relevant to perhaps the technologically and economically most important area of mechanochemistry, the reaction of additives in lubricants, known as tribochemistry. Such additives are crucial for preventing wear, lowering friction, preventing oxidation, and improving component lifetime.[26] It could also be viewed as a mechanocatalytic reaction in which surface chemistry and mechanical forces conspire to induce a reaction that would not occur in the absence of an external force.

Two distinct mechanically induced elementary reaction steps are identified. The first is the mechanochemical S−CH_3 bond cleavage of adsorbed methyl thiolate species, analogous to the single-molecule pulling experiments, except that, in this case, reaction is induced by the lateral and normal forces exerted on the mechanophore. Here, the methyl thiolate forms rapidly

Received: April 19, 2017
Accepted: July 14, 2017

DOI: 10.1021/acsami.7b05440
ACS Appl. Mater. Interfaces XXXX, XXX, XXX−XXX

from DMDS on copper by thermal S−S bond scission.[27] The second is sliding-induced surface-to-bulk transport of the resulting chemisorbed sulfur. This results in oxidation of the copper by sulfur, and the regeneration of available copper surface sites, thereby allowing the reaction to continue. The following paper explores whether the elementary thermal and mechanochemical reaction steps found for methyl thiolate overlayers on copper can completely describe the steady-state reaction between DMDS and copper.

The kinetics of the mechanochemical reaction are monitored in situ from the evolution in friction force as a function of the number of times that the surfaces is rubbed. A kinetic model, incorporating the elementary mechanochemical reaction steps described above, accurately reproduces the variation in friction force as a function of the number of times the sample is rubbed, as well as the total amount of sulfur in the bulk of the copper and its depth distribution.

Identifying these elementary mechanochemical reaction steps, and developing robust kinetic models will set the stage for understanding and predicting more complex mechanochemical reactions and synthetic methods.

RESULTS

The mechanochemical reaction between DMDS and copper is carried out on clean copper foils under controlled conditions in an ultrahigh vacuum (UHV) chamber by rubbing the sample with a tungsten carbide ball (using a normal load of 0.44 N with a sliding speed of 4×10^{-3} m/s at a temperature of 290 K) in the presence of DMDS. The reaction kinetics are monitored in situ from the evolution in friction coefficient (μ, the ratio of the lateral force to the normal force). The experiment was carried out as follows. A clean copper sample was initially rubbed in vacuo until μ decreased from its initial value of ∼0.8 to a constant value of ∼0.5, generally after ∼50 to 70 passes, to create a track ∼100 μm wide. Reaction was then initiated by pressurizing the chamber with 5×10^{-8} Torr of DMDS (where pressures are not corrected for the ionization gauge sensitivity) while rubbing was continued while monitoring μ. Since the friction coefficient had stabilized during initial rubbing of the clean copper, subsequent changes in friction coefficient are due to mechanochemical reactions taking place on the surface. The results are displayed in Figure 1 where the first scan corresponds to the time at which the chamber was pressurized after completion of the run-in period. The line in Figure 1 is a fit to the kinetic model and will be discussed in greater detail below.

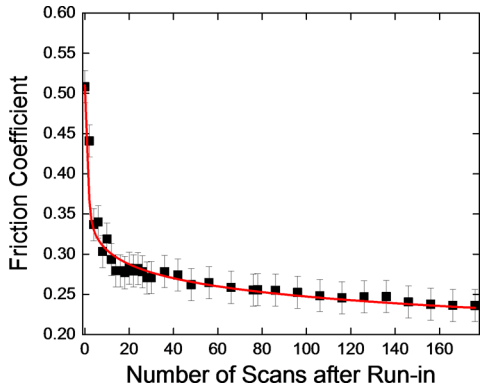

Figure 1. Plot of the friction coefficient μ as a function of the number of scans over a copper surface while sliding a tungsten carbide ball, after initially stabilizing μ (for ∼70 scans), and then allowing the sample to react with 5×10^{-8} Torr of DMDS under a normal load of 0.44 N at a sliding speed of 4×10^{-3} m/s at a sample temperature of 290 K. The results of the fit to the kinetic model are in red.

The friction coefficient initially decreases rapidly for ∼10 scans after introducing DMDS, then evolves at a much slower rate as rubbing continues. Because the friction coefficient is sensitive to the composition of the interface, this provides an in situ measurement of the mechanochemical reactions kinetics. The observation that μ evolves during the entire experiment indicates that a continuous mechanochemical reaction is taking place at the interface. As will be shown below, this is due to the transport of sulfur into the subsurface region, and the generation of surface reaction sites. Measurements of the resulting bulk sulfur accumulation are described in the next section.

Measurement of the Total Subsurface Sulfur. Bulk sulfur is measured quantitatively by taking advantage of the observation that subsurface sulfur is thermodynamically less stable than adsorbed sulfur. Thus, heating a sulfur-containing copper sample induces any subsurface sulfur to segregate to the surface, allowing the total amount of sulfur that had penetrated the subsurface region to be measured using Auger spectroscopy.[28] However, because the surface is covered by sulfur-containing adsorbates (adsorbed sulfur and methyl thiolate species) after carrying out the mechanochemical reaction, they are first carefully removed by Argon ion bombardment (∼120 s with a beam energy of 3 keV, 1 μA/cm^2). The point at which all surface sulfur-containing species had been removed is monitored by Auger spectroscopy by analyzing an unrubbed region of the surface.[28]

Subsequent heating to ∼750 K causes any subsurface sulfur to diffuse to the surface. The total amount of sulfur is measured by Auger spectroscopy using a focused electron beam (∼30 μm in diameter) by measuring the S(KLL)/Cu(LMM) Auger intensity ratio at various points across the sample where sulfur is detected. The integrated area of this curve is calibrated by comparing with similar plots of the S(KLL)/Cu(LMM) Auger intensity ratio causes by the removal of sulfur during sliding of a saturated methyl thiolate overlayer, where all the sulfur is mechanically removed from the rubbed region.[28] The experimental measurements of the total amount of subsurface sulfur versus the number of times that sample was rubbed in the presence of DMDS are shown in Figure 2(■). The solid line is a theoretical prediction based on the kinetic model described in the Discussion section.

Angle-Resolved Electron Spectroscopic Analyses of Subsurface Sulfur. The subsurface sulfur depth distribution is measured using angle-resolved X-ray photoelectron spectroscopy (XPS). Since the depth sensitivity in XPS is primarily dictated by the electron escape depth, and hence the electron mean-free path, varying the electron detection angle provides a nondestructive measure of the distribution of the subsurface sulfur.

Ex-situ angle-resolved XPS measurements of a rubbed region were made by transferring the sample from the UHV chamber via a nitrogen-filled glovebag to the XPS chamber, and then by removing any contaminant layer by Argon ion bombardment (∼42 s with a beam energy of 1 keV over an area of 3 × 3 mm^2). The resulting S 2p XPS spectra are displayed in Figure 3 as a function of emission angle, measured with respect to the surface, for a sample that had been rubbed 160 times. Corresponding spectra for samples that had been rubbed 40

DOI: 10.1021/acsami.7b05440
ACS Appl. Mater. Interfaces XXXX, XXX, XXX−XXX

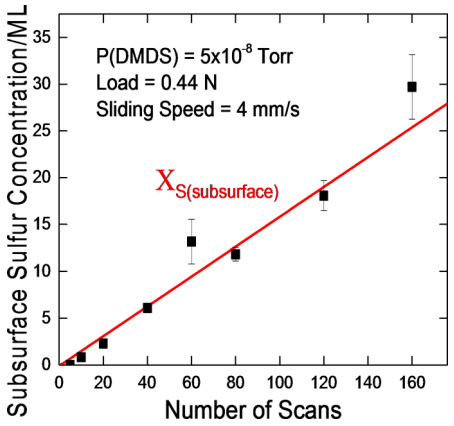

Figure 2. Plot of the total accumulated subsurface sulfur measured as a function of the number scans in the presence of 5×10^{-8} Torr of DMDS under a load of 0.44 N at a sliding speed of 4 mm/s at a sample temperature of 290 K. The solid line is the amount of subsurface sulfur calculated from the kinetic model and the subsurface sulfur concentration is given in units of monolayers (ML) of sulfur.

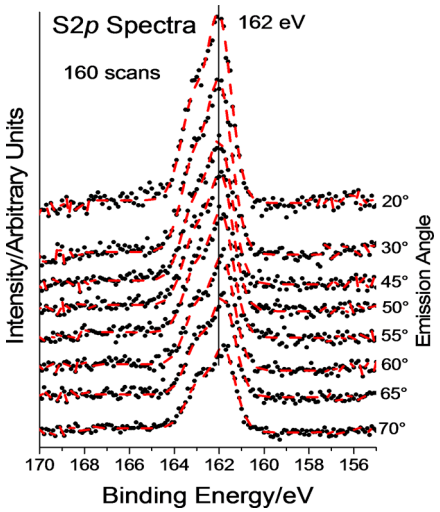

Figure 3. A series of small-spot-size S 2*p* angle-resolved XPS spectra inside the wear track after rubbing a clean copper sample after the completion of a run-in period in the presence of a background pressure of 5×10^{-8} Torr of dimethyl disulfide for 160 scans at a load of 0.44 N, a sliding speed of 4 mm/s at a sample temperature of 290 K. The spectra were collected at various emission angles, which are indicated adjacent to the corresponding spectrum.

and 80 times are shown in the Supporting Information (SI) section (Figure S1). The peak positions remain constant for different emission angles with a S $2p_{3/2}$ binding energy of 162.0 ± 0.1 eV. The depth distribution is obtained from the angular intensity variation by the maximum entropy method.[29] The results are shown in Figure S2, which confirm that sulfur has penetrated the subsurface region of the copper substrate.

A Cu $2p_{3/2}$ signal is detected at ~932.6 eV but cannot distinguish between metallic Cu and Cu_2S, while the Cu LMM Auger signal can be used to distinguish the chemical states of copper.[30−32] Figure 4 displays an example of the Cu LMM Auger signals after curve fitting (see SI for details) showing contributions to the Auger signal collected at 20° (Figure 4(a)) and 70° (Figure 4(b)) emission angles.

Metallic copper is in blue; its relative intensity decreases with emission angle consistent with sulfur penetrating the bulk since the higher the emission angle, the lower the sampling depth. An additional profile is fitted using the components of cuprous sulfide but by allowing the peak positions to vary slightly. The most intense peak for metallic copper ($CuL_3M_{45}M_{45}$ ^1G) is found at 918.6 eV kinetic energy (ref 32 and references therein), while the additional signal has the most intense peak at 917.1 ± 0.1 eV kinetic energy. For reference, the main Auger feature for Cu_2O is found at 916.8 ± 0.1 eV,[32] Cu_2S at 917.4,[33] and CuO at 917.8 ± 0.1 eV[32] kinetic energies.

DISCUSSION

It is proposed that the mechanochemical reaction between DMDS and copper proceeds via the follow elementary steps (Illustrated schematically in the Graphical Abstract): (i) Rapid dissociative adsorption of DMDS to form adsorbed methyl thiolates ($CH_3{-}S_{(ads)}$)[27] to provide an anchored mechanophore, (ii) mechanochemical S−CH_3 bond scission to evolve gas-phase hydrocarbons (methane and C_2 hydrocarbons)[34−38] and adsorbed sulfur, (iii) sliding-induced copper oxidation that regenerates clean surface sites.[28,35,38,39]

The first-order elementary-step reaction rate constants have been measured, both for step ii, methyl thiolate decomposition (k_1),[28,36,37] and step iii, shear-induced surface-to-bulk transport (k_2), under an identical load (0.44 N) and sliding speed (4 mm/s) at 290 K as for the experiments reported here. This limits the number of adjustable parameters in the kinetic model. In the absence of sliding, the thermal rate constants for both processes are negligible and methyl thiolate species and adsorbed sulfur are stable on the surface at 290 K; their rates are both mechanochemically accelerated. The kinetics are modeled in the following by assuming that mechanochemical reactions only occur when the surface of the moving ball is in contact with the substrate surface. The average time that a point on the surface spends in the sliding contact is designated t_C. This allows the kinetics equations to be written *as a function of the number of passes over the surface p* where the total reaction time t in the contact is given by $t = t_C p$. Since mechanical reactions were carried out at identical loads and sliding speeds, t_C remains constant. This yields first-order rate constants for overlayers of adsorbed thiolate species of $k_1 t_C = k_1' = 0.63 \pm 0.03$,[38] and $k_2 t_C = k_2' = 2.5 \pm 0.5$.[39] Note that these rate constants for mechanochemical reactions of methyl thiolate overlayers were measured under identical condition (normal load, 0.44 N, sliding speed 4 mm/s at 290 K) as used in the results presented here.

The pass-dependent coverage of the i^{th} surface species is designated $\Theta_i(p)$, where coverages are defined as the number of adsorbed species ratioed to the maximum number that can be accommodated, so that $0 \leq \Theta \leq 1$. To compare the results of the kinetic model with in situ experimental data (Figure 1), it is assumed that each (i^{th}) adsorbate has an associated characteristic friction coefficient μ_i, and that its contribution to the total friction is proportional to its coverage, so that the evolution of the friction coefficient as a function of the number of passes $\mu(p)$ is written as follows:[38]

$$\mu(p) = \sum_i \mu_i \Theta_i(p) \tag{1}$$

Characteristic friction coefficients for a methyl thiolate-covered (μ_{th}), sulfur-covered (μ_S) and a clean surface (μ_{clean}) are $\mu_{th} = 0.07 \pm 0.02$, $\mu_S = 0.39 \pm 0.06$, and $\mu_{clean} = 0.51 \pm 0.05$.[38] The possibility that the presence of sulfur in the subsurface can modify the friction of the substrate is taken into account by

DOI: 10.1021/acsami.7b05440
ACS Appl. Mater. Interfaces XXXX, XXX, XXX−XXX

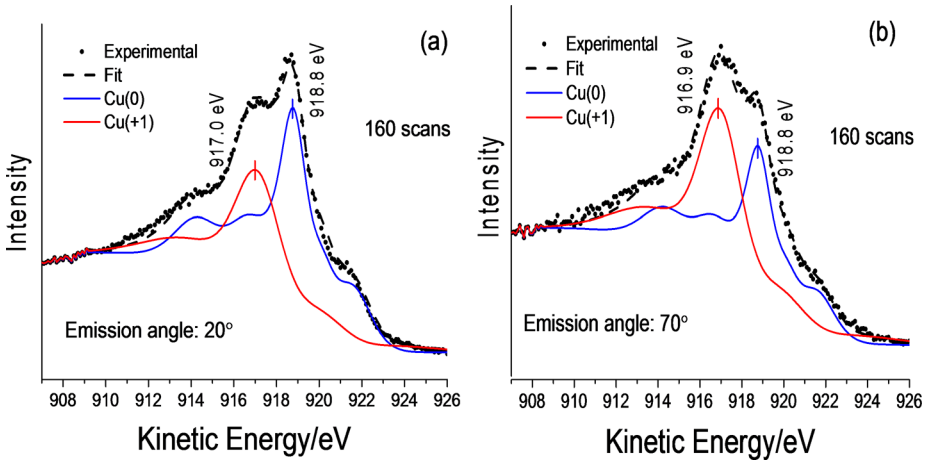

Figure 4. Cu KLL Auger spectra obtained within the rubbed region for a sample that had been rubbed for 160 scans in 5×10^{-8} Torr of DMDS at 290 K and then ion bombarded for 42 s to remove the contaminant layer, collected at detection angles of (a) 20° and (b) 70° with respect to the surface. Shown also are fitted Auger profiles.

including a characteristic friction coefficient for copper sites with subsurface sulfur, $\mu_{S(sub)}$. This value is not available, and will be used as an adjustable parameter.

The initial conditions for the simulation are set by assuming that DMDS initially reacts with copper prior to the first pass of the ball over the surface after exposure to DMDS to rapidly produce an initial methyl thiolate coverage, Θ_{th}^0. To help estimate both Θ_{th}^0 and the change in methyl thiolate coverage between each pass of the ball over the surface (see below), methyl thiolate adsorption kinetics were measured from the change in S(KLL)/Cu(LMM) Auger intensity ratio as a function of DMDS exposure. The results are displayed in Figure S3 as coverage (normalized to unity) versus exposure.

The kinetic equations for the elementary step reactions are solved iteratively as a function of the number of passes to yield values of the methyl thiolate coverage $\Theta_{th}(p)$, the sulfur coverage $\Theta_S(p)$, and the clean surface coverage, $\Theta_{clean}(p)$ where

$$\Theta_{th}(p) + \Theta_S(p) + \Theta_{clean}(p) = 1 \quad (2)$$

Note that the clean surface coverage is taken to represent the proportion of the surface at which DMDS can rapidly thermally react to form methyl thiolate species. It is assumed in the model that this can also occur on clean surface sites that contain sulfur in the layer below, with coverage $\Theta_{S(sub)}(p)$.

The calculation is started with an initial methyl thiolate coverage, Θ_{th}^0, taken as an adjustable parameter. The extent of reaction during each pass is calculated as follows: (i) the proportion of thiolate species that decomposes is calculated using a first-order mechanochemical reaction with rate constant k_1', (ii) Θ_S is calculated by assuming that each decomposing methyl thiolate species produces an adsorbed sulfur atom, (iii) $\Theta_{S(sub)}$ is obtained by assuming a first-order reaction with rate constant k_2', and the total amount of subsurface sulfur is found by summing this value for each sliding pass. Finally, Θ_{clean} is found from eq 2.

During the mechanochemical reaction, the pin slides for ~1s and comes out of contact, moves to the beginning of the rubbed region, and approaches the surface again to ensure that the loads are identical for all scans. This typically takes ~15 to 20 s, during which time a proportion P of the remaining clean copper surface (with coverage Θ_{clean}) becomes covered by methyl thiolate species, thus adding to any methyl thiolate species already on the surface from the previous pass. This defines the initial conditions for each pass and the extent of reaction is calculated as a function of p using the reaction steps described above.

The friction coefficient $\mu(p)$ is calculated from eq 1 as follows:

$$\mu(p) = \mu_{th}\Theta_{th}(p) + \mu_S\Theta_S(p) + \mu_{clean}(\Theta_{clean}(p) - \Theta_{S(sub)}) + \mu_{S(sub)}\Theta_{S(sub)} \quad (3)$$

where the coverage of clean copper sites without any subsurface sulfur is given by $(\Theta_{clean}(p) - \Theta_{S(sub)})$.

The values of Θ_{th}^0, $\Theta_{S(sub)}$ and P are adjusted to produce the best fit to the experiment measurement of friction coefficient as a function of the number of passes in Figure 1. The fit is shown as a solid line and yields $P = 0.39 \pm 0.02$, $\Theta_{th}^0 = 0.23 \pm 0.02$ and $\mu_{S(sub)} = 0.12 \pm 0.02$. The value of P is within the expected range (see Figure S3). Note that the value of $\mu_{S(sub)}$ is substantially lower than that for the clean surface ($\mu_{clean} = 0.51 \pm 0.05$) implying that subsurface sulfur does modify the friction of the copper.

The resulting evolution of the composition of the copper is shown as a function of number of passes in Figure 5. This reveals that the coverages of the adsorbed sulfur and methyl

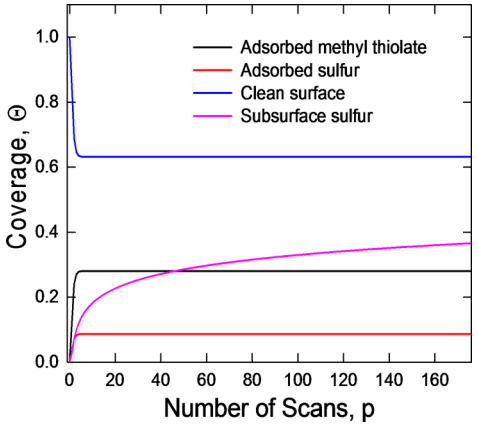

Figure 5. Plots of the calculated coverages of adsorbed methyl thiolate, sulfur, the clean surface and subsurface sulfur as a function of the number of passes using parameters that gave the best fit to the friction data (Figure 1).

DOI: 10.1021/acsami.7b05440
ACS Appl. Mater. Interfaces XXXX, XXX, XXX−XXX

thiolates vary during the first few scans, but rapidly reach steady-state values. This occurs when the number of methyl thiolate species that adsorb on the surface between each pass exactly balances those that mechanochemically decompose. As sliding continues, the total amount of bulk sulfur (present as S^{2-}, Figure 2) increases (Figure 5), thereby causing $\Theta_{S(sub)}$ to continuously increase. Since the clean surface coverage $\Theta_{clean}(p)$ remains constant, this indicates that the proportion of clean surface sites that contain no subsurface sulfur deceases during rubbing.

These observations rationalize the evolution in friction coefficient with the number of passes (Figure 1); the rapid initial decrease in friction coefficient is associated with the adsorption of methyl thiolate species and the formation of sulfur on the copper surface. Subsurface sulfur then starts to accumulate, giving rise to the continued, slow decrease in friction coefficient. Further details on the kinetic analysis are provided in SI Section S2.

Subsurface Sulfur Concentration and Distribution. The fit to the friction data depends only on three fitting parameters, namely of Θ^0_{th}, $\Theta_{S(sub)}$, and P, where the values of Θ^0_{th}, and P are constrained. However, the kinetic model makes a number of assumptions, in particular that methyl thiolate species can react on surface copper sites modified by sulfur below the surface. In order to further test the assumptions of the kinetic model, measurements of both the total amount of subsurface sulfur and its distribution within the sample are compared with predictions of the model. Note that assuming that methyl thiolate species formed only on clean sites without subsurface sulfur would lead to less sulfur penetrating the bulk of the sample.

The total amount of subsurface sulfur is calculated by summing the sulfur that is transported into the bulk during each cycle over all cycles (see SI Section S2). The prediction of the kinetic model (Figure 2, solid line) are compared with the experimental results (■), where the agreement is excellent, thus providing further verification of the mechanochemical reaction mechanism and the kinetic model.

The first-order kinetics of the sliding-induced transport of sulfur into the subsurface region, used in the above analysis, is equivalent to assuming that the distance that sulfur penetrates the sample is proportional to the number of times that it is rubbed.[35,39] Thus, if the distance that the sulfur penetrates into the bulk per pass is d_p, then, for a sulfur-covered surface that has been rubbed p times, surface sulfur penetrates a distance $z = pd_p$ into the bulk. When the sample is continuously dosed with DMDS, each sulfur overlayer will have been rubbed a different number of times. For example, a sulfur overlayer that was present during the first scan will have penetrated a distance pd_p into the sample, while an overlayer that was present during the second scan will have penetrated a distance $(p - 1)d_p$, and so on. The resulting sulfur depth distribution is the sum of all contributions arising from each scan and is illustrated schematically in Figure S4. This gives a subsurface sulfur concentration $C_S(p,z')$ given by the following:

$$C_S(p, z') = \frac{\Theta_S}{(k'_2)}\left(\ln\left(\frac{p}{z'}\right) - \frac{1}{2}\left(\frac{1}{p} - \frac{1}{z'}\right)\right) \quad (4)$$

where $z' = \frac{z}{d_p}$,[38] and the derivation of eq 4 is described in greater detail in SI Section S3. The solutions to eq 3 are plotted in Figure 6 for p = 40 (■), 80 (●), and 160 (▲) passes,

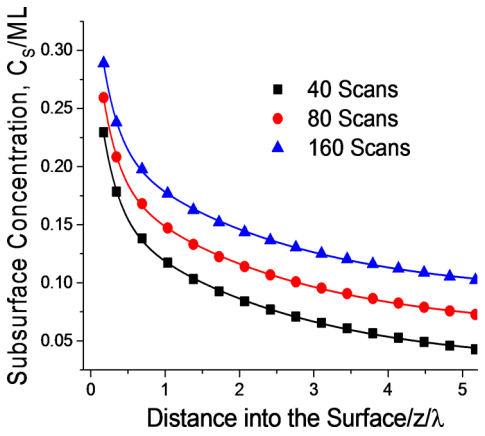

Figure 6. Plot of the subsurface sulfur concentration as a function of the total number of passes, 40 (black ■), 80 (red ●), and 160 (blue ▲), where the concentration is plotted in units of monolayers of sulfur (ML), and the depth, z, is ratioed to the electron mean free path λ for S 2p electrons with a kinetic energy of ~1320 eV when using an Al Kα source.

where the concentration is plotted in units of monolayers of sulfur (ML), and the depth, z, is ratioed to the electron mean free path λ for S 2p electrons with a kinetic energy of ~1320 eV when using an Al Kα source.[40] Thus, the deepest sulfur arises from that present on the surface early in the experiment, while the bulk sulfur closest to the surface is due to surface sulfur that was present toward the end of the experiment. The results indicate that the sulfur has penetrated a distance that is of the order of the mean-free path of the emitted electrons; angle-resolved XPS provides an ideal, nondestructive means of measuring the depth profile. The variation in the intensity of the S 2p XPS peak was calculated using the depth distributions in Figure 6, by assuming that the signal originating from some distance d in the sample at some emission angle Θ varies as $\exp\left(-\frac{d}{\lambda \cos \Theta}\right)$, where λ is the electron mean-free path. The resulting calculated angular variations of the S 2p intensities are shown in Figure 7 for samples that have been rubbed 40 (pink

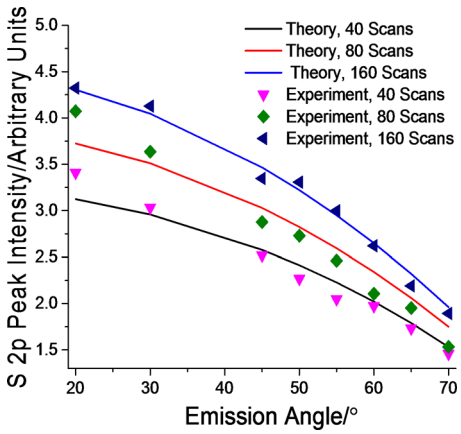

Figure 7. Plot of the integrated area of the S 2p XPS feature, taken from the data shown in Figures 3 and S1 as a function of emission angle measured with respect to the surface for a sample that had been rubbed 40 (pink ▼), 80 (green ♦), and 160 (blue ▲) times in 5 × 10^{-8} Torr of DMDS with a load of 0.44 N at 4 mm/s. The lines represent calculated variations in S 2p intensity as a function of detection angle after rubbing as discussed in the text.

DOI: 10.1021/acsami.7b05440
ACS Appl. Mater. Interfaces XXXX, XXX, XXX−XXX

▼), 80 (green ♦) and 160 (blue ▲) times in the presence of DMDS. Shown also plotted on this figure are the experimental data obtained from the spectra shown in Figures 3 and S1 for samples that had been rubbed 40 (▼), 80 (♦), and 160 (▲) times in 5×10^{-8} Torr of DMDS. The agreement between the theory and experiment is excellent.

Nature of the Subsurface Sulfur. The S 2*p* XPS (Figures 3 and S1) indicate that the sulfur oxidation state corresponds to a sulfide (S^{2-}) for all detection angles. This implies that the sulfur has the same oxidation state even though the Cu:S stoichiometry varies as a function of depth and the number of times that the surface has been rubbed (Figure 6).

The X-ray-induced Auger data (Figure 4) provide information on the chemical state of the copper. Metallic copper is evident from the major peak at 918.6 eV KE, and the lower relative intensity of this profile for grazing detection (Figure 4(b)) is in accord with the larger sulfur content near the sample surface (Figure 6). The additional intensity in the Auger spectra gives the best fit to a profile with the main peak centered at 917.0 ± 0.1 eV KE. Unlike XPS chemical shifts, the position of the main Auger feature does not vary monotonically with copper oxidation state so that, for example, the main peak for Cu_2O is found at 916.7 eV,[32] Cu_2S at 917.4,[33] and CuO at 918.7 eV KE. This does, however, indicate that a portion of the copper is oxidized, but has not yet formed a stoichiometric sulfide, suggesting the sulfide ions are uniformly distributed throughout the surface region of the copper rather than aggregating to form regions of stoichiometric sulfides.

The specific friction coefficient of the sample with subsurface sulfur is ∼0.12, somewhat higher than the value of friction coefficient for copper lubricated by DMDS dissolved in a poly α-olefin, where the friction coefficient was ∼0.05.[36] In this case, the conditions were more severe than those for the UHV experiments and may result in the formation of a complete cuprous sulfide film. However, the friction coefficient of cuprous sulfide has been found to depend on load and sliding velocity,[41] which may also account for differences between the values.

The kinetic model focuses on the mechanochemical processes occurring on the substrate in contact with a spherical pin sliding on it. In principle, changes could also occur on the pin itself during sliding. However, the pin is continually in contact with the sliding interface, so that the surface of the pin will react rapidly at the beginning of the scan to evolve to a steady-state condition. Furthermore, the surface analyses of the total amount of sulfur in the sample (Figure 2) and measurements of the sulfur depth distribution (Figure 7) suggest that any evolution in the state of the pin does not have a significant influence on the kinetic model and friction.

CONCLUSIONS

This work identifies two elementary-step mechanochemical processes, namely sliding-induced S−CH_3 bond scission and mechanochemical copper oxidation, and demonstrates that they completely account for the experimental reaction kinetics and the evolution in the amount of subsurface sulfur and its distribution. It should also be mentioned that surface temperatures can increase due to frictional heating to also accelerate rates of chemical reactions, and have been found to dominate film formation processes under severe conditions.[42−45] The temperature rise in these experiments was negligible, allowing such effects to be excluded.

Mechanistic studies such as those presented here will enable the physical origins of these elementary-step mechanochemical processes to be understood. For example, mechanochemical reactions induced by a sliding AFM tip have demonstrated that the reaction rate increases approximately exponentially with shear-stress[46] or contact pressure.[46,47] The underlying mechanisms for both mechanochemical reactions induced by sliding and single-molecule pulling experiments are identical. They are described in the mechanochemistry community by the Bell equation[48] and its variants.[49] In fact, the general physical concepts that describe the way in which an external force accelerates the rate of transition over an energy barrier were first presented at the beginning of the last century by Prandtl[50] and also used by Eyring to model fluid viscosity[51] as well as other mechanically induced processes.[52] They have also been used to describe nanoscale friction measured in the AFM[53−55] by the so-called Prandtl-Tomlinson model.[52,56] Molecular simulations have been carried out for alkyl thiolate species on coinage metal surfaces[21,24,57−59] to probe the molecular mechanisms occurring under normal and lateral stresses. Such theoretical studies have suggested that shear of alkyl thiolate-covered silver and gold can occur within the metal substrate and can result in the evolution of metal-containing species, not observed for a pin sliding over copper. Such studies are relevant to understanding the molecular origin of elementary mechanochemical reaction steps identified in this work.

The underpinnings of the surface-to-bulk transport processes have been described using molecular-dynamics simulations[60−62] and such processes and the resulting mechanically induced structural changes are likely to be applicable to many mechanochemical processes.

METHODS

Vacuum System. Mechanochemical measurements were carried out in a stainless-steel UHV chamber operating at a base pressure of $\sim 2 \times 10^{-10}$ Torr following bakeout, which has been described in detail elsewhere.[63] Briefly, the chamber was equipped with a UHV-compatible tribometer, which simultaneously measures the normal load, lateral force and contact resistance between the tip and substrate. Previous work has demonstrated that the maximum interfacial temperature rise for a copper sample under the experimental conditions used (4×10^{-3} m/s sliding speed, 0.44 N normal load) is much less than 1 K.[34]

All experiments were carried out by initially rubbing the tribopin (made of tungsten carbide covered by a copper transfer film) of 1.27×10^{-2} m in diameter against the clean copper sample until a constant friction coefficient was obtained. The sample, which was held at ∼290 K for all experiments, was dosed with DMDS through a leak valve connected to a dosing tube (with an internal diameter of 4×10^{-3} m) directed toward the sample so that the pressure at the sample surface is enhanced compared to the measured background pressure. The chamber was also equipped with a single-pass cylindrical-mirror analyzer (CMA) for Auger analysis, and an argon ion bombardment source for sample cleaning and depth profiling. A high-resolution electron gun with a beam energy of 5 keV, and a channeltron secondary electron detector, were also incorporated into the system. This allowed scanning electron microscopy (SEM) images and Auger spectra of the rubbed regions to be collected. Finally, the chamber also included a quadrupole mass spectrometer for leak checking, detecting gas-phase products formed during rubbing and for gauging reactant purity. The measurement procedures are described in greater detail in the SI Section S1.

XPS Measurements. XPS measurements were made by removing the samples from the UHV chamber in a nitrogen-filled glovebag and storing them in a sealed container under nitrogen. Further experimental details are provided in the SI Section S1.

DOI: 10.1021/acsami.7b05440
ACS Appl. Mater. Interfaces XXXX, XXX, XXX−XXX

Materials. The copper samples (Alfa Aesar, 99.99% pure, 1 mm thick) were polished to a mirror finish using 1 μm diamond paste and then rinsed with deionized water and ultrasonically degreased in acetone. Once in UHV, the copper foils were cleaned using a standard procedure, which consisted of Argon ion bombardment (~1 keV, ~2 $\mu A/cm^2$) and annealing cycles up to ~600 K for 300 s. The cleanliness of the samples was monitored using Auger spectroscopy.

The dimethyl disulfide (DMDS, Aldrich, 99.0% purity) was transferred to glass bottles and attached to the gas-handling systems of the vacuum chamber, where they were subjected to several freeze–pump–thaw cycles. The purity of the compounds was monitored using mass spectroscopy.

■ ASSOCIATED CONTENT

Supporting Information

The Supporting Information is available free of charge on the ACS Publications website at DOI: 10.1021/acsami.7b05440.

XPS spectra collected after 40 and 80 rubbing cycles, uptake curve of methyl thiolate species on the rubbed region, kinetic analysis of the mechanochemical reaction, and the subsurface sulfur distribution. Sulfur in-depth distributions in the various scars obtained by applying the MEM algorithm to the ARXPS data profile (PDF)

■ AUTHOR INFORMATION

Corresponding Author

*Tel: +1-414-229-5222. E-mail: wtt@uwm.edu (W.T.T.).

ORCID

Antonella Rossi: 0000-0002-5151-2634

Wilfred T. Tysoe: 0000-0002-9295-448X

Author Contributions

H.A., B.P.M., O.J.F., and Y.X. carried out tribological measurements, H.A. and Y.X. measured the subsurface sulfur concentration and prepared samples for XPS analysis, M.F. and A.R. carried out XPS measurements, processed and interpreted the data, G.N. applied the MEM to the ARXPS profiles, P.V.K. and W.T.T. performed the kinetic modeling, analyzed the data, and oversaw writing of the paper.

Notes

The authors declare no competing financial interest.

■ ACKNOWLEDGMENTS

We gratefully acknowledge support of the National Science Foundation under grants number CMMI-1265742 and CMMI-1634340. The authors wish to thank Prof. Nicholas D. Spencer for having allowed the access to the Quantera SXM; Dr. Andrea Arcifa and Mr. Cossu are acknowledged for the technical assistance. University of Cagliari is acknowledged for the financial contribution to this work.

■ REFERENCES

(1) Theophrastus, H. J. Theophrastus'S History of Stones: With an English Version and Critical and Philisophical Notes, Including the Modern History of the Gems &C., Described by That Author and of Many Others of the Native Fossils. *London*, **1774**.

(2) Faraday, M. M. J. K. *Chemical Manipulation: Being Instructions to Students inCchemistry on the Methods of Performing Experiments of Demonstration or of Research with Accuracy and Success*; Carey and Lea: Philadelphia, 1831.

(3) Do, J.-L.; Friščić, T. Mechanochemistry: A Force of Synthesis. *ACS Cent. Sci.* **2017**, *3*, 13–19.

(4) Sohma, J. Mechanochemistry of Polymers. *Prog. Polym. Sci.* **1989**, *14*, 451–596.

(5) Boldyrev, V. V.; Tkáčová, K. Mechanochemistry of Solids: Past, Present, and Prospects. *J. Mater. Synth. Process.* **2000**, *8*, 121–132.

(6) Levitas, V. I. High-pressure Mechanochemistry: Conceptual Multiscale Theory and Interpretation of Experiments. *Phys. Rev. B: Condens. Matter Mater. Phys.* **2004**, *70*, 184118.

(7) Beyer, M. K.; Clausen-Schaumann, H. Mechanochemistry: The Mechanical Activation of Covalent Bonds. *Chem. Rev.* **2005**, *105*, 2921–2948.

(8) Kipp, S.; Šepelák, V.; Becker, K. D. Mechanochemie: Chemie mit dem Hammer. *Chem. Unserer Zeit* **2005**, *39*, 384–392.

(9) Todres, Z. V. *Organic Mechanochemistry and Its Practical Applications*; Taylor&Francis: Boca Raton, FL, 2006.

(10) Rosen, B. M.; Percec, V. Mechanochemistry: A Reaction to Stress. *Nature* **2007**, *446*, 381–382.

(11) Varma, R. S. Greener" Chemical Syntheses using Mechanochemical Mixing or Microwave and Ultrasound Irradiation. *Green Chem. Lett. Rev.* **2007**, *1*, 37–45.

(12) Mitchenko, S. A. Mechanochemistry in Heterogeneous Catalysis. *Theor. Exp. Chem.* **2007**, *43*, 211–228.

(13) Craig, S. L. Mechanochemistry: A Tour of Force. *Nature* **2012**, *487*, 176–177.

(14) Bowmaker, G. A. Solvent-assisted Mechanochemistry. *Chem. Commun.* **2013**, *49*, 334–348.

(15) Groote, R.; Jakobs, R. T. M.; Sijbesma, R. P. Mechanocatalysis: Forcing Latent Catalysts into Action. *Polym. Chem.* **2013**, *4*, 4846–4859.

(16) Makarov, D. E. Perspective: Mechanochemistry of Biological and Synthetic Molecules. *J. Chem. Phys.* **2016**, *144*, 030901.

(17) Urakaev, F. K.; Boldyrev, V. V. Mechanism and Kinetics of Mechanochemical Processes in Comminuting Devices: 1. Theory. *Powder Technol.* **2000**, *107*, 93–107.

(18) Urakaev, F. K.; Boldyrev, V. V. Mechanism and Kinetics of Mechanochemical Processes in Comminuting Devices: 2. Applications of the Theory. Experiment. *Powder Technol.* **2000**, *107*, 197–206.

(19) Duwez, A.-S.; Cuenot, S.; Jerome, C.; Gabriel, S.; Jerome, R.; Rapino, S.; Zerbetto, F. Mechanochemistry: Targeted Delivery of Single Molecules. *Nat. Nanotechnol.* **2006**, *1*, 122–125.

(20) Liang, J.; Fernandez, J. M. Mechanochemistry: One Bond at a Time. *ACS Nano* **2009**, *3*, 1628–1645.

(21) Konôpka, M.; Turanský, R.; Dubecký, M.; Marx, D.; Štich, I. Molecular Mechanochemistry Understood at the Nanoscale: Thiolate Interfaces and Junctions with Copper Surfaces and Clusters. *J. Phys. Chem. C* **2009**, *113*, 8878–8887.

(22) Ribas-Arino, J.; Marx, D. Covalent Mechanochemistry: Theoretical Concepts and Computational Tools with Applications to Molecular Nanomechanics. *Chem. Rev.* **2012**, *112*, 5412–5487.

(23) Klukovich, H. M.; Kouznetsova, T. B.; Kean, Z. S.; Lenhardt, J. M.; Craig, S. L. A Backbone Lever-arm Effect Enhances Polymer Mechanochemistry. *Nat. Chem.* **2012**, *5*, 110–114.

(24) Seema, P.; Behler, J.; Marx, D. Force-induced Mechanical Response of Molecule-metal Interfaces: Molecular Nanomechanics of Propanethiolate Self-assembled Monolayers on Au(111). *Phys. Chem. Chem. Phys.* **2013**, *15*, 16001–16011.

(25) Konda, S. S. M.; Brantley, J. N.; Varghese, B. T.; Wiggins, K. M.; Bielawski, C. W.; Makarov, D. E. Molecular Catch Bonds and the Anti-Hammond Effect in Polymer Mechanochemistry. *J. Am. Chem. Soc.* **2013**, *135*, 12722–12729.

(26) Holmberg, K.; Andersson, P.; Erdemir, A. Global Energy Consumption due to Friction in Passenger Cars. *Tribol. Int.* **2012**, *47*, 221–234.

(27) Furlong, O. J.; Miller, B. P.; Li, Z.; Walker, J.; Burkholder, L.; Tysoe, W. T. The Surface Chemistry of Dimethyl Disulfide on Copper†. *Langmuir* **2010**, *26*, 16375–16380.

(28) Furlong, O.; Miller, B.; Tysoe, W. Shear-Induced Surface-to-Bulk Transport at Room Temperature in a Sliding Metal–Metal Interface. *Tribol. Lett.* **2011**, *41*, 257–261.

(29) Scorciapino, M. A.; Navarra, G.; Elsener, B.; Rossi, A. Nondestructive Surface Depth Profiles from Angle-Resolved X-ray Photoelectron Spectroscopy Data Using the Maximum Entropy

DOI: 10.1021/acsami.7b05440
ACS Appl. Mater. Interfaces XXXX, XXX, XXX–XXX

Method. I. A New Protocol. *J. Phys. Chem. C* **2009**, *113*, 21328−21337.
(30) Castle, J. E. Auger Electron Spectroscopy. *Corrosion Technology* **2005**, *22*, 39−63.
(31) Wagner, C. D.; Muilenberg, G. E. *Handbook of X-ray Photoelectron Spectroscopy: A Reference Book of Standard Data for use in X-ray Photoelectron Spectroscopy. Physical Electronics Divison*; Perkin-Elmer Corp.: Eden Prairie, MN, 1979.
(32) Cocco, F.; Elsener, B.; Fantauzzi, M.; Atzei, D.; Rossi, A. Nanosized Surface Films on Brass Alloys by XPS and XAES. *RSC Adv.* **2016**, *6*, 31277−31289.
(33) Fantauzzi, M.; Atzei, D.; Elsener, B.; Lattanzi, P.; Rossi, A. XPS and XAES Analysis of Copper, Arsenic and Sulfur Chemical State in Enargites. *Surf. Interface Anal.* **2006**, *38*, 922−930.
(34) Adams, H. L.; Garvey, M. T.; Ramasamy, U. S.; Ye, Z.; Martini, A.; Tysoe, W. T. Shear-Induced Mechanochemistry: Pushing Molecules Around. *J. Phys. Chem. C* **2015**, *119*, 7115−7123.
(35) Furlong, O. J.; Miller, B. P.; Tysoe, W. T. Shear-Induced Surface-to-Bulk Transport at Room Temperature in a Sliding Metal-Metal Interface. *Tribol. Lett.* **2011**, *41*, 257−261.
(36) Furlong, O. J.; Miller, B. P.; Kotvis, P.; Tysoe, W. T. Low-Temperature, Shear-Induced Tribofilm Formation from Dimethyl Disulfide on Copper. *ACS Appl. Mater. Interfaces* **2011**, *3*, 795−800.
(37) Furlong, O.; Miller, B.; Tysoe, W. T. Shear-induced Boundary Film Formation from Dialkyl Sulfides on Copper. *Wear* **2012**, *274*−*275*, 183−187.
(38) Adams, H.; Miller, B. P.; Kotvis, P. V.; Furlong, O. J.; Martini, A.; Tysoe, W. T. In Situ Measurements of Boundary Film Formation Pathways and Kinetics: Dimethyl and Diethyl Disulfide on Copper. *Tribol. Lett.* **2016**, *62*, 1−9.
(39) Miller, B.; Furlong, O.; Tysoe, W. The Kinetics of Shear-Induced Boundary Film Formation from Dimethyl Disulfide on Copper. *Tribol. Lett.* **2013**, *49*, 39−46.
(40) Seah, M. P.; Dench, W. A. Quantitative Electron Spectroscopy of Surfaces: A Standard Data Base for Electron Inelastic Mean Free Paths in Solids. *Surf. Interface Anal.* **1979**, *1*, 2−11.
(41) Varenberg, M.; Ryk, G.; Yakhnis, A.; Kligerman, Y.; Kondekar, N.; McDowell, M. T. Mechano-Chemical Surface Modification with Cu_2S: Inducing Superior Lubricity. *Tribol. Lett.* **2016**, *64*, 28.
(42) Kotvis, P. V.; Huezo, L. A.; Tysoe, W. T. Surface Chemistry of Methylene Chloride on Iron - A Model for Chlorinated Hydrocarbon Lubricant Additives. *Langmuir* **1993**, *9*, 467−474.
(43) Kotvis, P. V.; Tysoe, W. T. Surface Chemistry of Chlorinated Hydrocarbon Lubricant additives - Part I: Extreme-pressure Tribology. *Tribol. Trans.* **1998**, *41*, 117−123.
(44) Blunt, T. J.; Kotvis, P. V.; Tysoe, W. T. Surface Chemistry of Chlorinated Hydrocarbon Lubricant Additives - Part II: Modeling the Tribological Interface. *Tribol. Trans.* **1998**, *41*, 129−139.
(45) Blunt, T. J.; Kotvis, P. V.; Tysoe, W. T. Determination of Interfacial Temperatures under Extreme Pressure Cconditions. *Tribol. Lett.* **1996**, *2*, 221−230.
(46) Felts, J. R.; Oyer, A. J.; Hernández, S. C.; Whitener, K. E., Jr; Robinson, J. T.; Walton, S. G.; Sheehan, P. E. Direct Mechanochemical Cleavage of Functional Groups from Graphene. *Nat. Commun.* **2015**, *6*, 6467.
(47) Gosvami, N. N.; Bares, J. A.; Mangolini, F.; Konicek, A. R.; Yablon, D. G.; Carpick, R. W. Mechanisms of Antiwear Tribofilm Growth Revealed In Situ by Single-Asperity Sliding Contacts. *Science* **2015**, *348*, 102−106.
(48) Bell, G. Models for the Specific Adhesion of Cells to Cells. *Science* **1978**, *200*, 618−627.
(49) Konda, S. S. M.; Brantley, J. N.; Bielawski, C. W.; Makarov, D. E. Chemical Reactions Modulated by Mechanical Stress: Extended Bell Theory. *J. Chem. Phys.* **2011**, *135*, 164103−8.
(50) Prandtl, L. Ein Gedankenmodell zur kinetischen Theorie der festen Körper. *Z. Angew. Math. Mech.* **1928**, *8*, 85.
(51) Eyring, H. Viscosity, Plasticity, and Diffusion as Examples of Absolute Reaction Rates. *J. Chem. Phys.* **1936**, *4*, 283−291.
(52) Spikes, H.; Tysoe, W. On the Commonality Between Theoretical Models for Fluid and Solid Friction, Wear and Tribochemistry. *Tribol. Lett.* **2015**, *59*, 1−14.
(53) Gnecco, E.; Bennewitz, R.; Gyalog, T.; Loppacher, C.; Bammerlin, M.; Meyer, E.; Güntherodt, H. J. Velocity Dependence of Atomic Friction. *Phys. Rev. Lett.* **2000**, *84*, 1172−1175.
(54) Gnecco, E.; Bennewitz, R.; Gyalog, T.; Meyer, E. Friction Eexperiments on the Nanometre Scale. *J. Phys.: Condens. Matter* **2001**, *13*, R619−R642.
(55) Bennewitz, R.; Gnecco, E.; Gyalog, T.; Meyer, E. Atomic Friction Studies on Well-defined Surfaces. *Tribol. Lett.* **2001**, *10*, 51−56.
(56) Dong, Y.; Vadakkepatt, A.; Martini, A. Analytical Models for Atomic Friction. *Tribol. Lett.* **2011**, *44*, 367−386.
(57) Seema, P.; Behler, J.; Marx, D. Peeling by Nanomechanical Forces: A Route to Selective Creation of Surface Structures. *Phys. Rev. Lett.* **2015**, *115*, 036102.
(58) Konôpka, M.; Turanský, R.; Reichert, J.; Fuchs, H.; Marx, D.; Štich, I. Mechanochemistry and Thermochemistry are Different: Stress-Induced Strengthening of Chemical Bonds. *Phys. Rev. Lett.* **2008**, *100*, 115503.
(59) Zoloff Michoff, M. E.; Ribas-Arino, J.; Marx, D. Nanomechanics of Bidentate Thiolate Ligands on Gold Surfaces. *Phys. Rev. Lett.* **2015**, *114*, 075501.
(60) Rigney, D. A. Transfer, Mixing and Associated Chemical and Mechanical Processes During the Sliding of Ductile Materials. *Wear* **2000**, *245*, 1−9.
(61) Kim, H.; Kim, W.; Falk, M.; Rigney, D. MD Simulations of Microstructure Evolution during High-Velocity Sliding between Crystalline Materials. *Tribol. Lett.* **2007**, *28*, 299−306.
(62) Karthikeyan, S.; Agrawal, A.; Rigney, D. A. Molecular Dynamics Simulations of Sliding in an Fe−Cu Tribopair System. *Wear* **2009**, *267*, 1166−1176.
(63) Gao, F.; Kotvis, P. V.; Tysoe, W. T. The Friction, Mobility and Transfer of Tribological Films: Potassium Chloride and Ferrous Chloride on Iron. *Wear* **2004**, *256*, 1005−1017.

DOI: 10.1021/acsami.7b05440
ACS Appl. Mater. Interfaces XXXX, XXX, XXX−XXX